Nonlinear Wave Making Resistance Calculation for Large Ships in Restricted Waterways

Xin Zhao[1,2*], Xujin Zhang[3]
[1]College of River and Ocean Engineering, Chongqing Jiaotong University, Chongqing 400074 China
[2]School of Hydraulic Engineering, Sichuan Water Conservancy Vocational College, Chengdu 611230, China
[3]Southwest Water Conservancy and Water Transport Engineering Research Institute, Chongqing Jiaotong University, Chongqing 400010, China
E-mail: zhaoxn0606@163.com
[*]Corresponding author

Keywords: ship, navigation channel, wave making, resistance value, FA-SSA, CFD

Received: May 22, 2024

The development of the maritime transportation industry has led to more frequent use of large ships, but they are affected significantly by wave making resistance during navigation. In order to improve the performance of the calculation model of wave making resistance of large ships, a hybrid optimization algorithm FA-SSA is constructed by combining firefly algorithm and squirrel search algorithm. By introducing the luminance and attraction mechanism of fireflies, the algorithm enhances the global and local search ability of squirrel search algorithm. Then, based on FA-SSA and computational fluid dynamics, a new calculation model of ship wave making resistance is established. The experimental results show that in the performance comparison of the hybrid optimization algorithm, the F-value and G-value of FA-SSA reached 85.2% and 92.3%, respectively, which was significantly better than other comparison algorithms, reflecting its high efficiency in solving complex optimization problems. Further, in the comparison experiment of the ship wave making resistance calculation model, the mean memory consumption of the proposed model was only 883.3Mb, and the error value was as low as 0.0086, which is significantly better than the traditional model, and the calculation accuracy and efficiency are significantly improved. The above results show that the model can accurately and efficiently calculate the nonlinear wave making resistance value of large ships on restricted waterways, which is of great value to promote the development of maritime transportation industry

Povzetek: Članek uvaja hibridni FA-SSA model za izračun upora pri valovanju velikih ladij v omejenih plovnih poteh, kar izboljša učinkovitost pomorskega transporta.

1 Introduction

With the increasing prosperity of global trade, the role of large ships in maritime transportation industry has become increasingly important [1]. However, large ships are full of risks in restricted waterways. The resistance generated by ship wave making poses significant risks to its economy and safety [2]. In restricted waterways, due to water depth limitations and constraints on both sides, ship wave making exhibits complex nonlinear characteristics [3]. This nonlinear wave making not only affects the stability of the ship navigation, but also leads to turbulence in the waterway, thereby increasing the navigation resistance [4]. Accurately calculating the nonlinear wave making resistance value of large ships in restricted waterways is of practical significance for improving navigation efficiency and ensuring navigation safety [5]. However, the current calculation accuracy of nonlinear wave making resistance values for large ships is relatively low. Therefore, it is crucial to find a new method for calculating the nonlinear wave making resistance value of large ships to improve the calculation accuracy. The development of numerical simulation techniques such as Computational Fluid Dynamics (CFD) has provided new methods for the research of ship wave making resistance [6]. CFD can simulate the wave making characteristics of ships under different channel conditions by constructing precise numerical models, and then analyze the mechanism and variation law of resistance generated. In addition, the machine learning technology has also provided ideas for optimizing the calculation method of ship wave making resistance. Therefore, this study innovatively combines machine learning technology with CFD. Then a new ship wave making resistance calculation model based on the two is constructed. It is expected that this method can improve the ship wave making resistance calculation accuracy, thereby promoting the development of maritime transportation. The research is divided into five parts. The first part reviews the knowledge of mechanics, machine learning, and research related to ships. The second part constructs the hybrid optimization algorithm and the new

ship wave making resistance calculation model. The third part compares and analyzes the hybrid optimization algorithm and the new ship wave resistance calculation model. The fourth part is the discussion and prospect of the research results and models. The fifth part is a summary of the entire text.

2 Related works

With the widespread application of mechanics knowledge in various fields, the branch of mechanics, fluid mechanics, has been widely applied. For example, Brunton combined fluid dynamics technology and machine learning technology into a data-driven model to propose an efficient and accurate data-driven model. Empirical analysis showed that the driving model had strong practicality, which was far superior to traditional driving models [7]. In addition, Cai et al. proposed a network structure based on fluid dynamics and physical information to better incorporate noisy data into existing algorithms. The results showed that the network structure had good application effects in incorporating noisy data into existing algorithms, with relatively low cost [8]. Machine learning is an interdisciplinary field that involves multiple complex disciplines. With the development of computer technology, its application areas are also becoming increasingly broad. For example, Greener et al. proposed a bio-informatics prediction model based on machine learning technology to address the difficulty of predicting information in biological processes. The results showed that the prediction accuracy was 98.3%, which was much higher than comparison models [9]. To improve the detection efficiency of structural damage and defects in civil engineering, Flah et al. proposed a structural health monitoring system based on machine learning algorithms. The actual application effects showed that the structural health monitoring system could effectively accurately monitor structural damage and defects in civil engineering, thereby improving the safety of civil engineering [10].

With the development of the maritime transportation industry, scholars have increasingly diversified their research on ships. For example, Song et al. used REGAL ordinary cargo ships to optimize the performance of full-size ships to test the dynamic performance of ships more accurately. The results showed that the optimized full-scale ship performance simulation experiment had a testing accuracy of 97.8% for ship dynamic performance, significantly better than before improvement [11]. In addition, the specific relationship between the roughness of the hull and the frictional resistance of the ship cannot be accurately predicted. Therefore, Song et al. proposed a groove test method based on flat plates and model ships. Experimental research was conducted on roughness and ship resistance using this method. The results showed that this method had good predictive performance and practicality [12]. To better quantify the forward uncertainty of ship engineering problems, Piazzola et al. proposed a multi fidelity method based on multi-index random configuration and adaptive multi-fidelity random radial basis functions. From the results, it could accurately quantify the forward uncertainty of ship engineering problems, which was helpful for the development of the ship engineering [13]. In addition, Feng et al. proposed a parameter optimization model based on full parameter modeling to improve the wave making resistance of ships. The model was used to optimize the ship and obtain the optimal hull. It was found that the wave making resistance of the optimal hull was significantly improved compared with before optimization. This result indicated that the proposed parameter optimization model had highly practical [14].

The results of the above related studies are summarized and presented in Table 1.

Table 1: Summary of related work and research results

Study	Method	Data set/application object	Key result	The shortcomings of SOTA
Brunton's data-driven model [7]	Fluid mechanics technology + machine learning	Data-driven model	Efficient and accurate data-driven model that outperforms traditional models	Not specifically targeted for specific applications in the maritime transportation
The network structure of Cai [8]	Networks of fluid mechanics and physical information	Noise data	Good inclusion of noise data, low cost	Without special research on nonlinear wave making resistance of large ships
Greener bio-informatics prediction model [9]	Machine learning technique	Bio-informatics data	The prediction accuracy is 98.3%, much higher than the comparison model	Application areas are not ships

Flah's Structural Health monitoring system [10]	Machine learning algorithm	Structural data of civil engineering	Effectively and accurately monitor structural damage in civil engineering	Application field is non-ship, lack of monitoring of ship structural health
Song for full size ship performance optimization [11]	REGAL general cargo ship experiment	Full-scale ship performance testing	The test accuracy is 97.8%, which is better than before the improvement	The calculation of nonlinear wave making resistance is not involved
Song's trench test method [12]	Experiments based on plates and ship models	Relationship between hull roughness and resistance	It has good predictive performance and practicability	Only the relationship between hull roughness and resistance is studied
Piazzola's multi-fidelity approach [13]	Multi-index random configuration and adaptive multi-fidelity method	Forward uncertainty of Marine engineering problems	Quantify positive uncertainty accurately	The application to ship resistance calculation is not mentioned
Feng's parameter optimization model [14]	Full parameter modeling	Optimization of hull anti-wave capability	The ability to withstand waves has been improved significantly	Limited to increasing the wave resistance of the vessel, not involving resistance calculation

From Table 1, although fluid mechanics and machine learning are widely used in their respective fields, there are relatively few applied studies in ship nonlinear wave making resistance calculation. The current state of the art technology lacks accurate calculation methods for nonlinear wave making resistance of large ships. In addition, although relevant studies have made progress in ship performance optimization, the relationship between hull roughness and resistance, and ship structural health monitoring, these studies have not directly solved the nonlinear wave making resistance calculation. Therefore, the current needs to fill the gap. Therefore, the research innovatively combines fluid mechanics and machine learning algorithm. Then it is applied to the nonlinear wave making resistance calculation of large ships, so as to improve the nonlinear wave making resistance calculation accuracy of large ships. This not only helps to promote the technological development of the ship field, but also enhances the integration and application effect of artificial intelligence and physical technology in the ship field.

3 Construction of nonlinear wave making resistance calculation model for large ships based on FA-SSA

To better calculate the nonlinear wave making resistance for large ships, this chapter first mixes the Firefly Algorithm (FA) and Squirrel Search Algorithm (SSA) to obtain the FA-SSA. Then, a new ship wave making resistance value calculation model is constructed based on the FA-SSA and CFD. It is expected that the calculation model can accurately calculate the nonlinear wave making resistance value for ships, thereby improving the navigation efficiency and safety.

3.1 Hybrid optimization algorithm combining FA and SSA

SSA is a novel and powerful global swarm intelligence optimization algorithm [15]. It originates from the natural foraging behavior of flying squirrels on various trees in the forest. Its workflow is shown in Figure 1.

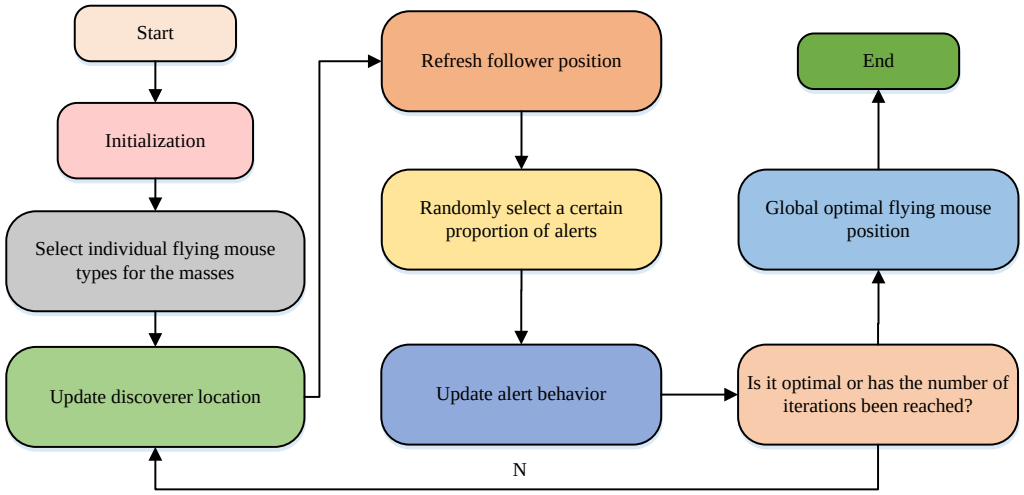

Figure 1: Flow chart of the SAA work

When initializing the SSA, the number of squirrels is set to FS. A uniform distribution is used to evenly distribute the position of each squirrel. The initialization is shown in Equation (1).

$$FS_{i,j} = FS + U(0,1) \times (FS_U - FS_L) \quad (1)$$

In Equation (1), $FS_{i,j}$ represents the position of the i-th squirrel in the j-th dimension. FS_U represents the upper boundary of the squirrel position. FS_L represents the lower boundary. $U(0,1)$ represents a random value within the [0,1]. The position of each squirrel after uniform distribution is random, and each squirrel's position represents a vector. All squirrel positions are shown in the matrix, as shown in Equation (2).

$$FS = \begin{bmatrix} FS_{1,1} & FS_{1.2} & \ldots & FS_{1,m} \\ FS_{2,1} & FS_{2.2} & \ldots & FS_{2,m} \\ \ldots & \ldots & \ldots & \ldots \\ FS_{n,1} & FS_{n,2} & \ldots & FS_{n,m} \end{bmatrix} \quad (2)$$

In Equation (2), each squirrel can freely change its position to search for food to search for the optimal solution. Because squirrels have individual differences, even in the same environment, the quantity and quality of food obtained by each squirrel are not necessarily the same. Therefore, the fitness of squirrels in the environment can be determined by the quantity and quality of food obtained by each squirrel. The fitness of squirrels is shown in Equation (3).

$$FS = \begin{bmatrix} f_1 & ([FS_{1,1} & FS_{1.2} & \ldots & FS_{1,m}]) \\ f_2 & ([FS_{2,1} & FS_{2.2} & \ldots & FS_{2,m}]) \\ & \ldots & \ldots & \ldots & \ldots \\ f_n & ([FS_{n,1} & FS_{n,2} & \ldots & FS_{n,m}] \end{bmatrix} \quad (3)$$

In this algorithm, the food sources of squirrels are divided into three types: excellent, moderate, and average. The three types of food sources correspond to the optimal solution, sub-optimal solution, and feasible solution, respectively. The fitness results obtained from Equation (3) are queued in ascending order. Squirrels with low fitness are located on superior food sources. Squirrels with moderate fitness are located on moderate food sources and tend to fly towards superior food sources. Squirrels with high adaptability are located on general food sources. In addition, all squirrels that meet their food needs tend to fly towards superior food sources, while squirrels that do not meet their food needs tend to fly towards moderate food sources. At the same time, all squirrels adjust their direction towards the food source based on the probability of predators appearing. Squirrel position adjustment is called position update. There are three main types of location updates. The first type is squirrels flying from a moderate food source to a superior food source, with the position update as shown in Equation (4).

$$FS_{at}^{t+1} = \begin{cases} FS_{at}^{t} + d_g \times G_c \times \left(FS_{ht}^{t} - FS_{at}^{t}\right) rand \geq P_{dp} \\ Random \quad location \quad otherwise \end{cases} \quad (4)$$

In Equation (4), FS_{at} represents the squirrel position on moderate food sources. FS_{ht} represents the squirrel position on premium food sources. d_g represents the sliding step length. G_c represents the squirrel sliding constant. t represents the number of iterations. P_{dp} represents the probability of predators appearing. The second type is squirrels flying from general food sources to moderate food sources, with the position update as shown in Equation (5).

$$FS_{nt}^{t+1} = \begin{cases} FS_{nt}^{t} + d_g \times G_c \times \left(FS_{at}^{t} - FS_{nt}^{t}\right) rand \geq P_{dp} \\ Random \quad location \quad otherwise \end{cases} \quad (5)$$

In Equation (5), FS_{nt} represents the squirrel

position on general food sources. FS_{at} represents the squirrel position on moderate food sources. *rand* represents a random value within [0, 1]. The third type is squirrels flying from general food sources to superior food sources. The position update is shown in Equation (6).

$$FS_{nt}^{t+1} = \begin{cases} FS_{nt}^{t} + d_g \times G_c \times \left(FS_{ht}^{t} - FS_{nt}^{t} \right) rand \geq P_{dp} \\ Random \quad location \quad otherwise \end{cases} \tag{6}$$

In Equation (6), FS_{nt} represents the squirrel position on general food sources. FS_{ht} represents the squirrel position on premium food sources. Although SSA has good optimization ability, it has problems such as being easily trapped in local optimal solutions, and lack of universality and flexibility [16]. Therefore, FA is used to optimize it. The brightness attraction mechanism and adaptability of FA are used to improve the local search ability and flexibility of SSA. FA is a heuristic algorithm inspired by the flickering behavior of fireflies [17]. The flashing behavior of fireflies can serve as a signaling system, aiming to attract other fireflies. The principle of FA is shown in Figure 2 [18]

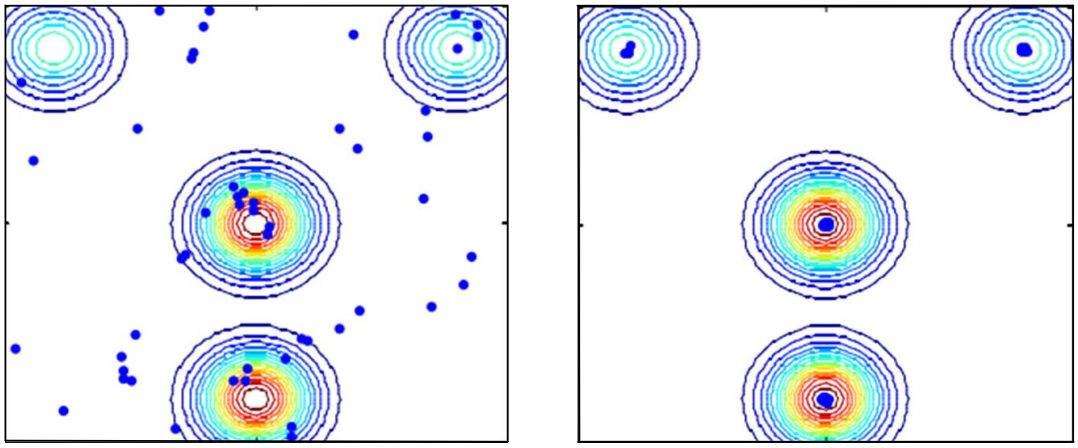

(a) Initial population distribution of fireflies

(b) Images of the distribution of fireflies after they gather

Figure 2: Schematic diagram of firefly algorithm

In Figure 2, when fireflies emit fluorescence, surrounding fireflies are attracted by the fluorescence. Because the brightness of the fluorescence emitted by each firefly varies, and the firefly moves towards the firefly that emits brighter fluorescence, all fireflies will eventually gather near the firefly that emits brighter fluorescence. The relative fluorescence brightness of fireflies is shown in Equation (7).

$$I = I_0 \times e^{-\gamma r_{ab}} \tag{7}$$

In Equation (7), I_0 represents the fluorescence brightness of fireflies. I_0 represents the objective of the corresponding optimization problem. The higher fluorescence brightness indicates a larger target value. γ is the light intensity absorption coefficient, which can reflect the different fluorescent brightness corresponding to different propagation media and moving distance. r_{ab} is the distance between firefly individuals a and b, and its expression is shown in Equation (8).

$$r_{ab} = \left| x_a - x_b \right| = \sqrt{\sum_{k=1}^{d} (x_{ak} - x_{bk})^2} \tag{8}$$

In Equation (8), x_a represents the spatial location of firefly a. x_b is the spatial location where firefly b is located. In addition, the attraction of fireflies is shown in Equation (9).

$$\beta = \beta_0 \times e^{\gamma r_{ab}{}^2} \tag{9}$$

In Equation (9), β represents the attraction of fireflies. β_0 represents the maximum attraction. When firefly a is attracted by firefly b and moves towards the firefly b, the position update of firefly a is shown in Equation (10).

$$x_i = x_i + \beta \times (x_b - x_a) + \sigma \times (rand - 1/2) \tag{10}$$

In Equation (10), σ and *rand* represent the movement step factor and random factor of fireflies, respectively. The study improves the SSA through the FA to improve its search efficiency. The improved FA-SSA can continue to search for the optimal solution at local extremes. The running process of this hybrid algorithm is shown in Figure 3

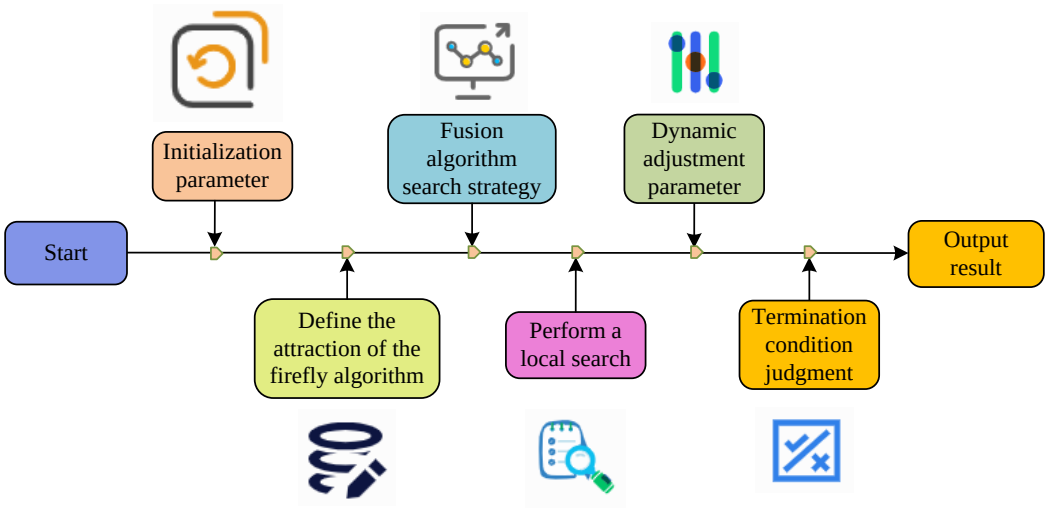

Figure 3: Running flow of FA-SSA

FA-SSA combines the brightness and attraction mechanism of FA with the search strategy of SSA to improve the solving efficiency of global optimization problems. The detailed operation process of the algorithm is as follows. Firstly, the algorithm parameters are initialized, including population size, number of iterations and brightness attenuation coefficient, etc., and the location and speed of the squirrel population are randomly generated. Then, each squirrel's fitness value is calculated to assess its performance. In the main loop, the algorithm first introduces the brightness and attraction from FA, guiding the search direction by calculating the brightness of each squirrel and the attraction between them. The squirrel's position and speed are then updated based on attraction and brightness information, combined with randomness and perturbation mechanisms. After each iteration, the local search is performed to further explore potential better solutions near the current optimal solution. At the same time, the algorithm dynamically adjusts its parameters according to the feedback information in the search process to optimize the search process. When the termination condition is satisfied, the algorithm stops iterating and outputs the optimal solution and its corresponding fitness value.

3.2 Construction of ship wave making resistance calculation model combining improved FA-SSA and CFD

CFD has emerged with the development of computer technology and numerical calculation techniques [19]. The basic principle of CFD is to numerically solve the differential equations that control fluid flow, obtain the discrete distribution of the fluid flow field in a continuous region, and approximately simulate fluid flow [20]. The basic flowchart of CFD is shown in Figure 4.

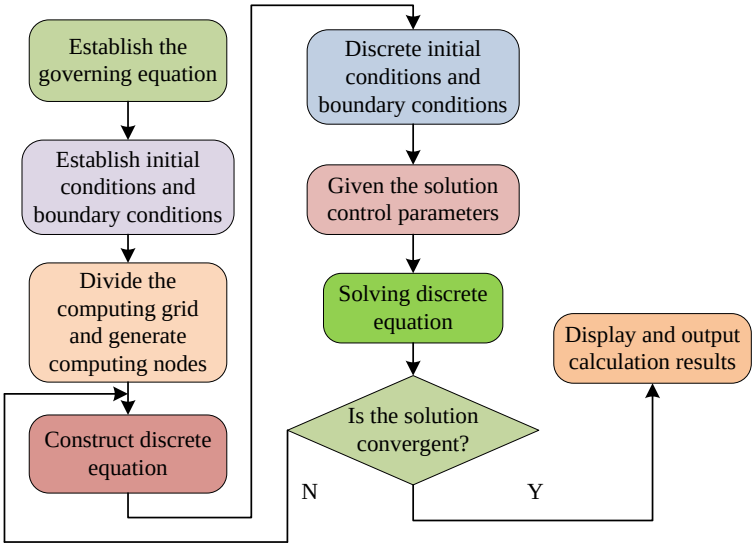

Figure 4: Basic flow chart of CFD operation

In Figure 4, CFD first establishes the control equation. The general form of the control equation is shown in Equation (11).

$$\frac{\partial(\rho\phi)}{\partial t}+\nabla\cdot(\rho u\phi)=\nabla\cdot(\Gamma\nabla\phi)+S \tag{11}$$

In Equation (11), ϕ represents a universal variable. ρ and u represent fluid density and velocity vectors, respectively. Γ and S represent diffusion coefficients and source terms, respectively. Then, based on the control equation, the initial and boundary conditions are determined. Secondly, the computational grid is divided, computing nodes are generated, and discrete equations are established. The discrete equation is shown in Equation (12).

$$\frac{\phi_m^{n+1}-\phi_m^n}{\Delta t}=\frac{\Gamma}{\Delta x^2}(\phi_m^{n+1}-2\phi_m^n+\phi_{m-1}^n) \tag{12}$$

In Equation (12), ϕ_i^n represents the variable value at time n and spatial point m. Δt and Δx represent time and space steps, respectively. Subsequently, the discretization initial and boundary conditions of the discrete equation are determined. The control parameters for solving the discrete equation are provided. If the obtained solution converges, the calculation result is finally output. If the obtained solution does not converge, the discrete equation is re-established for calculation. The commonly used convergence criterion is based on residual variation, which is the difference between the actual solution and the previous iteration solution. Therefore, the convergence criterion is shown in Equation (13).

$$\frac{\left\|\phi^{n+1}-\phi^n\right\|}{\left\|\phi^n\right\|}<\varepsilon \tag{13}$$

In Equation (13), ε represents the acceptable error limit. When the ratio of residual to solution is less than ε, it indicates that the solution has converged. The calculation method of ship wave making resistance is important research in the ship engineering. This study proposes a CFD-based ship wave making resistance calculation model, which accurately predicts the wave making resistance generated by ships during navigation through the CFD, providing strong support for ship design and optimization. When constructing the CFD-based model for calculating ship wave making resistance, a three-dimensional geometric model of the ship is first established. It is meshed, discretizing the ship surface and surrounding fluid into a large number of computational units. The constructed three-dimensional geometric model of a large ship is shown in Figure 5.

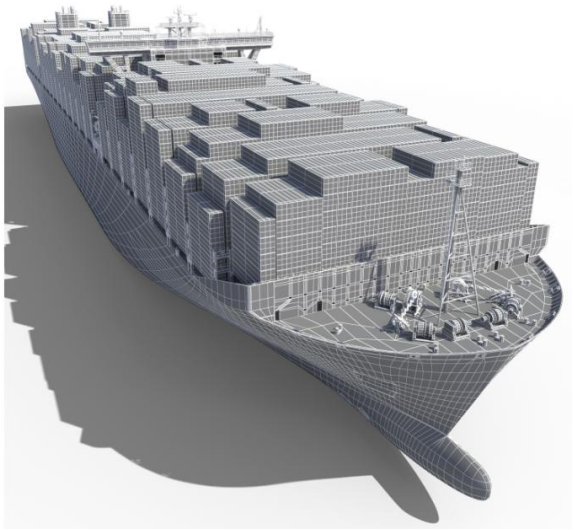

Figure 5: 3D geometric model of large ship

Secondly, based on the fluid control equation, combined with appropriate initial and boundary conditions, the motion equation of the ship in the fluid is constructed. The fluid control equation used in the study is the Navier-Stokes equation, which is expressed as Equation (14).

$$\frac{\partial u}{\partial t}+(u\cdot\nabla)u=-\frac{1}{\rho}\nabla p+v\nabla^2u+g \tag{14}$$

In Equation (14), ∂u represents the velocity vector of the fluid. ρ and p represent fluid density and pressure, respectively. u and g represent kinematic viscosity and gravitational acceleration, respectively. In addition, considering the nonlinear effects of fluids, this computational model adopts high-order numerical methods for solving, ensuring the accuracy and stability of the calculation results. Finally, key data such as the wave making resistance coefficient and waveform of the ship are obtained through post-processing of the calculation results, providing intuitive reference for ship

designers. The wave making resistance coefficient is shown in Equation (15).

$$C_w = \frac{R_w}{0.5\rho V^2 S} \tag{15}$$

In Equation (15), $0.5\rho V^2$ represents the dynamic pressure. S represents the wet surface area of the ship. C_w and R_w represent the wave making resistance coefficient and the ship wave making resistance, respectively. Although the CFD-based ship wave making resistance calculation model can effectively calculate the wave making resistance, there are still shortcomings in terms of computational efficiency and global optimization. Therefore, this study utilizes the FA-SSA to optimize the parameters in the CFD-based ship wave making resistance calculation model to improve its computational efficiency and global optimization ability. The specific process of the proposed ship wave making resistance calculation model that integrates the FA-SSA and CFD is shown in Figure 6.

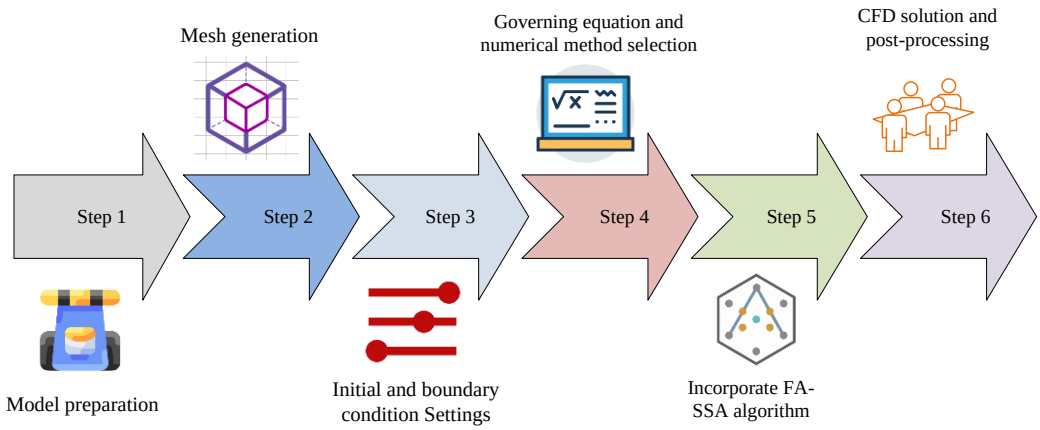

Figure 6: Flow of ship wave resistance calculation model combining FA-SSA and CFD

From Figure 6, the integration of CFD and FA-SSA first needs to determine the three-dimensional geometry of the hull, and lays the foundation for subsequent analysis by establishing an accurate three-dimensional CAD model. Then, the CFD model is prepared, which includes simulating the computational domain size and boundary conditions of the real marine environment, as well as using CFD processing software to finely mesh the ship surface and computational domain. After setting the initial and boundary conditions of the CFD model, the appropriate governing equation is selected for solving. Before solving the CFD equation, FA-SSA algorithm is introduced to optimize the key parameters in the CFD model. The optimization process is similar to that of FA-SSA, but the optimization goal is to find the model parameters that make the CFD calculation results optimal. After the optimization is completed, the CFD equation is solved according to the best parameters obtained, and the calculated results are post-processed to extract key data such as wave making resistance coefficient and waveform. Finally, the results are analyzed deeply to evaluate the rationality of hull design and navigation performance, which provides strong support for marine engineering practice.

4 Performance comparison of the improved optimization algorithm and empirical analysis of the resistance calculation model

To analyze the application effect of the FA-SSA proposed in the study, this chapter conducts comparative experiments on four optimization algorithms on the CEC dataset and BBOB dataset to demonstrate the high performance of the FA-SSA. In addition, a comparative experiment is conducted on the ship wave making resistance calculation model in this chapter. The experimental results demonstrate the superiority of the proposed model for calculating ship wave making resistance.

4.1 Performance verification of improved FA-SSA

To verify the performance of the FA-SSA, it is first validated on the CEC competition function dataset. The test results of the FA-SSA on the training and testing sets are shown in Figure 7.

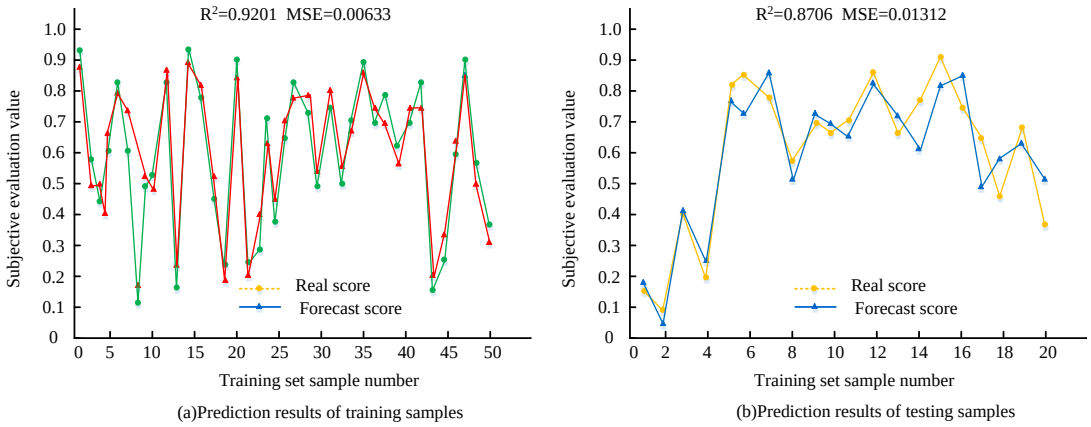

Figure 7: Test results of training set and testing set

From Figure 7 (a), the square correlation coefficient value of the FA-SSA in the training set was 0.9201, and the mean square error was 0.00633. The above two data indicate that the FA-SSA has high fitness in the training set, with strong generalization ability in the training set. According to Figure 7 (b), the square correlation coefficient and mean square error of the FA-SSA in the testing samples were 0.8706 and 0.01312, respectively. The above results indicate that the FA-SSA performs well in both the training and testing sets. To verify the effectiveness of the FA-SSA, comparative experiments are conducted with SSA, GA-SSA, and GA-FA on Matlab simulation software. Convergence, G-value, and F-value are used as comparison indicators for performance comparison. The comparison results of the convergence curves of the four algorithms on the CEC competition function dataset and the BBOB dataset are shown in Figure 8.

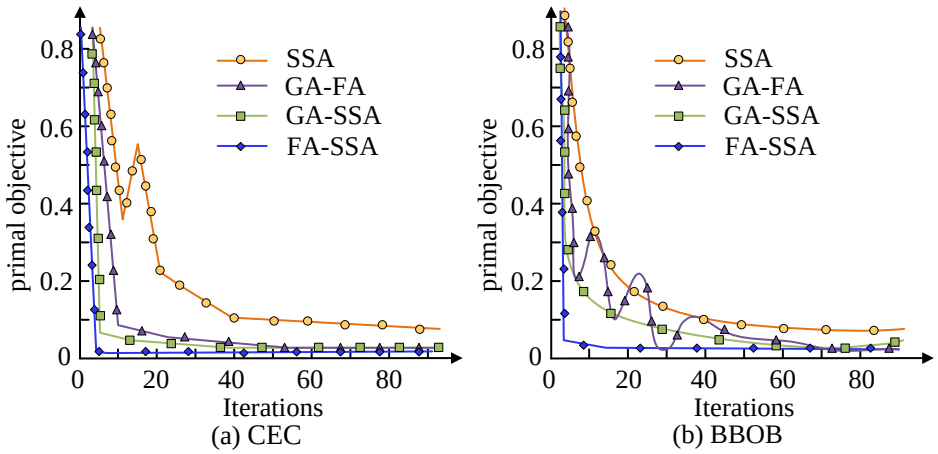

Figure 8: Comparison of convergence curves of different algorithms

From Figure 8 (a), the FA-SSA had the best convergence in the CEC dataset, reaching its optimal convergence at 5 iterations, which was far superior to other comparison algorithms. Moreover, the convergence curve of this algorithm was stable, with little fluctuation. From Figure 8 (b), compared with other algorithms in the BBOB dataset, the FA-SSA had the fastest convergence speed, reaching its optimal convergence at 3 iterations. The convergence speed of FA-SSA was 31.8 times, 22.9 times, and 21.6 times faster than SSA, GA-FA, and GA-SSA, respectively. From the above results, the performance of the FA-SSA is significantly better than that of the comparison algorithms. Finally, performance analysis is conducted by comparing the F-value and G-value of the four algorithms. The experimental results of the F-value and G-value of the four algorithms are shown in Figure 9.

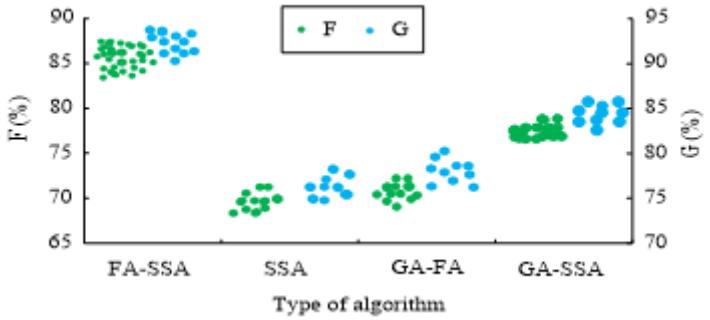

Figure 9: F-value and G-value of the four algorithms

In Figure 9, the F-value of the FA-SSA was concentrated around 85%. The SSA was concentrated around 67%. The GA-FA was concentrated around 73%. The GA-SSA was concentrated around 78%. In addition, from Figure 9, the G-value of FA-SSA, SSA, GA-FA, and GA-SSA was approximately 92.3%, 76.5%, 77.2%, and 84.1%. High F-value and G-value indicate better performance of the algorithm. The F-value and G-value of the FA-SSA are higher than those of comparison algorithms. Therefore, the overall performance of the FA-SSA is better than other comparison algorithms. Finally, in order to verify the wide applicability and robustness of the FA-SSA, two benchmark datasets IEEE CEC 2017 and IEEE CEC 2020 are added to the CEC and BBOB datasets. These two datasets contain different types of complex optimization problems, which can comprehensively evaluate the performance of the algorithm. Table 2 shows the performance comparison results between FA-SSA and other three comparison algorithms (SSA, GA-FA, GA-SSA) on four benchmark datasets. The number of convergence iterations, the mean value of the optimal solution, the standard deviation and the results of statistical significance test are listed in Table 2. The P-value represents the T-test P-value between FA-SSA and other algorithms on the mean value of the optimal solution. When the P-value is less than 0.05, it indicates that the difference is significant.

Table 2: Performance comparison on four algorithm benchmark datasets

Data set	Algorithm	Convergence iterations	The mean of the optimal solution	Standard deviation	P
CEC 2013	FA-SSA	5	0.00633	0.00015	/
	SSA	16	0.01021	0.00023	<0.001
	GA-FA	12	0.00874	0.00019	<0.001
	GA-SSA	10	0.00756	0.00017	<0.001
BBOB	FA-SSA	3	0.00210	0.00005	/
	SSA	96	0.00682	0.00018	<0.001
	GA-FA	72	0.00543	0.00012	<0.001
	GA-SSA	68	0.00581	0.00015	<0.001
IEEE CEC 2017	FA-SSA	7	0.00456	0.00011	/
	SSA	21	0.00789	0.00020	<0.001
	GA-FA	17	0.00623	0.00014	<0.001
	GA-SSA	14	0.00598	0.00013	<0.001
IEEE CEC 2020	FA-SSA	6	0.00321	0.00008	/
	SSA	19	0.00567	0.00016	<0.001
	GA-FA	15	0.00482	0.00012	<0.001
	GA-SSA	12	0.00423	0.00010	<0.001

From Table 2, FA-SSA outperformed other comparison algorithms on the four benchmark datasets. FA-SSA not only converges quickly, but also performs well in the mean value and stability of the optimal solution. From T-test, the difference between FA-SSA and other algorithms was statistically significant ($P<0.001$), which proved the wide applicability and robustness of FA-SSA for solving different types of complex optimization problems. Its excellent performance makes FA-SSA have great potential in practical applications.

4.2 The actual effect verification of nonlinear wave making resistance calculation model

After verifying the performance superiority of the proposed FA-SSA, the application effect of the wave making resistance calculation model based on FA-SSA and CFD was compared with other commonly used methods, including the proposed wave making resistance calculation model (Model 1), CFD-based wave making resistance calculation model (Model 2), and the wave making resistance calculation model based on machine learning algorithm (Model 3). The data of large ships on restricted waterways are collected as the dataset for this comparative experiment. The large ship calculation grid and free-liquid surface waveform used in the dataset are shown in Figure 10.

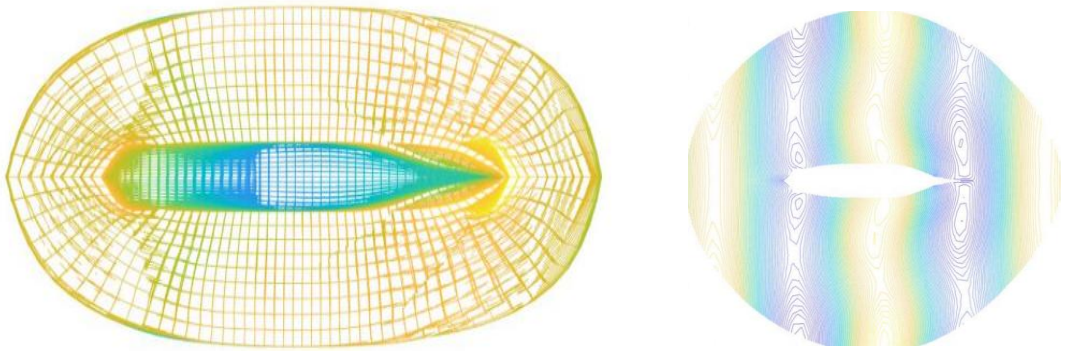

(a) Large ship computing domain grid (b) Free liquid surface waveform diagram

Figure 10: Calculation grid and free-liquid surface waveform of large ships

The prediction error results of the three models in this dataset are shown in Figure 11.

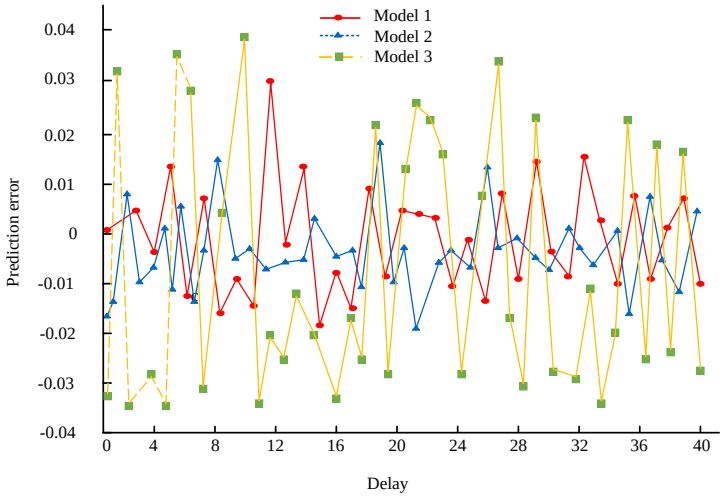

Figure 11: Calculation error results of the three models in this dataset

From Figure 11, the overall error of Model 1 was better than that of Model 2 and Model 3. The maximum error value of Model 1 was 0.019, Model 2 was 0.025, and Model 3 was 0.038. The deigned method was significantly better than comparison methods. The calculation error value of Model 1 was mostly in the range of -0.01 to 0.01, with little overall fluctuation. Furthermore, in Figure 11, the mean error of Model 1 was 0.0086, significantly lower than 0.013 of Model 2 and 0.019 of Model 3. From the perspective of calculation error, Model 1 performs better than comparison models. In addition, the study also statistically analyzes the computational time and consumption of the three models, as displayed in Table 3.

Table 3: Comparison of the computing time, memory consumption, and CPU usage of the three models

Test serial number	Model class	Computing time (s)	Memory consumption (MB)	CPU usage (%)
1	Model 1	68	878	60.5
	Model 2	536	4125	95.3
	Model 3	122	1533	75.8
2	Model 1	65	883	59.6
	Model 2	551	4156	94.8
	Model 3	118	1563	76.2
3	Model 1	66	889	61.2
	Model 2	562	4218	95.8
	Model 3	119	1486	74.9

According to Table 3, in all three experiments, Model 1 had the lowest computational time, with a mean computational time of 66.3 s, model 2 was 549.7 s, and model 3 was 119.7 s. Comparatively speaking, the method proposed in the study is significantly lower. In addition, the mean memory consumption and CPU usage of Model 1 were 883.3 Mb and 60.4%, respectively, which were significantly lower than comparison models. The above results indicate that the overall computational consumption of Model 1 is better than Model 2 and Model 3, which is more practical in the nonlinear wave making resistance calculation of ships. Finally, the correlation analysis is used to compare the computational accuracy of the three models. The correlation analysis results of the three models are shown in Figure 12.

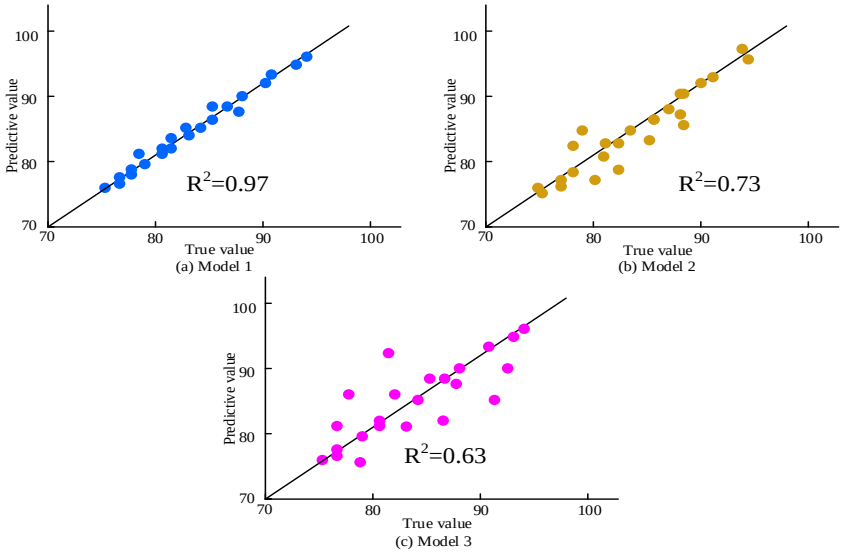

Figure 12: Prediction accuracy of different models

In Figure 12 (a), Model 1 had a high computational accuracy, with an R2 of 0.97. In Figure 12 (b), the calculation accuracy of Model 2 was moderate, with an R2 of 0.73. In Figure 12 (c), the calculation accuracy of Model 3 was relatively low, with an R2 of 0.63. Based on the comprehensive comparison of Figures 12 (a), (b), and (c), the computational accuracy of Model 1 is significantly better than that of Model 2 and Model 3. This result indicates that the proposed model also has good computational performance. Based on the above dimensions, the computational efficiency and computational consumption of the proposed model are

better than those of the comparison models, which is at a relatively high level.

5 Discussion

5.1 Comparison between FA-SSA and other optimization methods

The results show that FA-SSA has significant advantages in convergence speed and accuracy. Compared with SSA, GA-FA, GA-SSA and other optimization algorithms, FA-SSA performs better than comparison algorithms on multiple benchmark datasets such as CEC, BBOB, IEEE CEC 2017, and IEEE CEC 2020. Among them, FA-SSA performs well in the convergence speed. For example, it only took 5 iterations to achieve optimal convergence on CEC dataset, while it only took 3 iterations on BBOB dataset, and its convergence speed was tens of times that of SSA, GA-FA and GA-SSA respectively. In addition, FA-SSA also performs well in the mean value and stability of the optimal solution, with F-value and G-value significantly higher than other algorithms, which proves the efficiency and robustness of FA-SSA in solving complex optimization problems. This result is consistent with the results obtained by XX et al. [21]. The reason for this difference is that FA-SSA combines the brightness and attraction mechanism of FA with the search strategy of SSA. The brightness and attraction mechanism of FA provides the algorithm with global search capability, while the search strategy of SSA enhances the local search capability. The combination enables FA-SSA to quickly locate the approximate location of the optimal solution on a global scale, and fine-tune the quality of the solution through the local search strategy, thus achieving fast and high-precision convergence.

5.2 Improvement of calculation model efficiency and accuracy

The research results also showed that compared with the traditional CFD method, the wave making resistance calculation Model (Model 1) based on FA-SSA and CFD improved the calculation efficiency and accuracy. This result is similar to the conclusion obtained by XX team [22]. Although traditional CFD methods can accurately simulate fluid flow, the computational cost is high, especially when dealing with complex geometry and large-scale computing domains, which consumes a lot of computing time and resources. In Model 1, FA-SSA is introduced to optimize the key parameters in the CFD model, which significantly reduces the calculation cost. As shown in Table 3, the mean computation time of Model 1 was only 66.3s, compared with 549.7s for the Model 2, while memory consumption and CPU usage were also significantly reduced. In terms of accuracy, the Model 1 also performs well. As shown in Figure 11, the maximum error value of Model 1 was 0.019, which was significantly lower than that of Model 2 (0.025) and Model 3 (0.038), and the mean error was only 0.0086. This shows that Model 1 effectively reduces computing cost and improves computing efficiency while maintaining high accuracy. This improvement is mainly due to the FA-SSA algorithm accurately optimizing the parameters of the CFD model, allowing the model to more accurately simulate fluid flow during the calculation process, thereby improving the accuracy of the calculation results.

5.3 Explanation of the new method combining FA-SSA and CFD

The method combining FA-SSA with CFD to calculate wave making resistance is an innovative attempt. This method makes use of the advantages of FA-SSA in global optimization and the accuracy of CFD in fluid simulation. By optimizing the parameters of CFD model through the algorithm, the computational efficiency and accuracy are improved. FA-SSA first optimizes key parameters such as turbulence model coefficient and boundary layer treatment in CFD model, so that the model can be closer to the actual flow situation in the calculation process. Then, the optimized CFD model is used to calculate the wave making resistance, and the accurate result is obtained. This combination method not only improves the calculation efficiency, but also guarantees the accuracy of the calculation results, providing a new method for the wave making resistance calculation in the field of marine engineering.

5.4 Potential practical applications and limitations

The proposed model has broad potential practical applications in the field of marine engineering. Especially in the calculation of wave resistance for large ships navigating in restricted waters, this model can accurately predict wave resistance and provide strong support for ship design and optimization. In addition, the model can also be applied to other fluid dynamics problems, such as ship maneuverability, sea-keeping etc. However, there are some limitations to this model. First of all, the accuracy and efficiency of the model are affected by the algorithm parameters and the complexity of the CFD model, which needs to be adjusted and optimized according to the specific situation in practical applications. Secondly, the adaptability of the model to complex geometry and extreme flow conditions needs to be further verified and improved. In order to give full play to the potential of this model, future research can focus on the following aspects. The first is to further optimize the algorithm parameters and CFD model to improve the accuracy and efficiency of the model. The second is to carry out more experimental verification and case studies to evaluate the applicability of the model in different scenarios. The third is to explore the application potential of the model in other fluid dynamics problems and broaden the application range of the model.

6 Conclusion

In response to the insufficient accuracy in the wave making resistance calculation model for large ships today, an improved ship wave making resistance calculation model that integrated intelligent optimization algorithms and CFD was proposed. The study first constructed a wave making resistance calculation model based on CFD, and then optimized the parameters of CFD using AF-SSA to obtain an improved ship wave making resistance calculation model. In the comparative experiment of AF-SSA, the convergence speed of the FA-SSA was 31.8 times, 22.9 times, and 21.6 times faster than that of the SSA, GA-FA, and GA-SSA, respectively. Afterwards, performance tests were conducted on the proposed ship wave resistance calculation model in a nonlinear wave dataset. The results showed that the mean error of the proposed model was 0.0086, significantly lower than 0.013 of Model 2 and 0.019 of Model 3. The above results indicate that the improved the wave making resistance calculation model has higher accuracy in calculating the nonlinear wave making resistance of ships. Therefore, it can be applied to calculate the nonlinear wave making resistance of large ships in restricted waterways, providing data support for formulating appropriate optimization strategies. In addition, the validation dataset for the study is single. In the future, more data needs to be selected for experiments to demonstrate the universality of the model.

Fundings

The research is supported by: This work was supported by National Key R&D Plan Project (No.2016YFC0402006).

References

[1] T. P. Sapsis, “Statistics of extreme events in fluid flows and waves,” Annual Review of Fluid Mechanics, vol. 53, no. 1, pp. 85-111, 2021. https://doi.org/10.1146/annurev-fluid-030420-032810

[2] N. Kapilan, P. Vidhya, and X. Z. Gao, “Virtual laboratory: A boon to the mechanical engineering education during covid-19 pandemic,” Higher Education for the Future, vol. 8, no. 1, pp. 31-46, 2021. https://doi.org/10.1177/2347631120970757

[3] R. D. Moser, S. W. Haering, and G. R. Yalla, “Statistical properties of subgrid-scale turbulence models,” Annual Review of Fluid Mechanics, vol. 53, no. 1, pp. 255-286, 2021. https://doi.org/10.1146/annurev-fluid-060420-023735

[4] P, P. Groumpos, “A critical historic overview of artificial intelligence: issues, challenges, opportunities, and threats,” Artificial Intelligence and Applications, vol. 1, no. 4, pp. 197-213, 2023. https://doi.org/10.47852/bonviewAIA3202689

[5] J. Purohit, and R. Dave, “Leveraging deep learning techniques to obtain efficacious segmentation results,” Archives of Advanced Engineering Science, vol. 1, no. 1, pp. 11-26, 2023. https://doi.org/10.47852/bonviewAAES32021220

[6] B. Liu, M. Ding, S. Shaham, W. Rahayu, F. Farokhi, and Z. Lin, “When machine learning meets privacy: A survey and outlook,” ACM Computing Surveys (CSUR), vol. 54, no. 2, pp. 1-36, 2021. https://doi.org/10.1145/3436755

[7] S. L. Brunton, “Applying machine learning to study fluid mechanics,” Acta Mechanica Sinica, vol. 37, no. 12, pp. 1718-1726, 2021. https://doi.org/10.1007/s10409-021-01143-6

[8] S. Cai, Z. Mao, Z. Wang, M. Yin, and G. E. Karniadakis, “Physics-informed neural networks (PINNs) for fluid mechanics: A review,” Acta Mechanica Sinica, vol. 37, no. 12, pp. 1727-1738, (2021). https://doi.org/10.1007/s10409-021-01148-1.

[9] J. G. Greener, S. M. Kandathil, L. Moffat, and D. T. Jones, “A guide to machine learning for biologists,” Nature Reviews Molecular Cell Biology, vol. 23, no. 1, pp. 40-55, 2022. https://doi.org/10.1038/s41580-021-00407-0

[10] M. Flah, I. Nunez, W. Ben Chaabene, and M. L. Nehdi, “Machine learning algorithms in civil structural health monitoring: A systematic review,” Archives of computational methods in engineering, vol. 28, no. 4, pp. 2621-2643, 2021. https://doi.org/10.1007/s11831-020-09471-9

[11] K. Song, C. Guo, C. Sun, C. Wang, J. Gong, P. Li, and L. Wang, “Simulation strategy of the full-scale ship resistance and propulsion performance,” Engineering Applications of Computational Fluid Mechanics, vol. 15, no. 1, pp. 1321-1342, 2021. https://doi.org/10.1080/19942060.2021.1974091

[12] S. Song, S. Dai, Y. K. Demirel, M. Atlar, S. Day, and O. Turan, “Experimental and theoretical study of the effect of hull roughness on ship resistance,” Journal of Ship Research, vol. 65, no. 01, pp. 62-71, 2021. https://doi.org/10.5957/JOSR.07190040

[13] C. Piazzola, L. Tamellini, R. Pellegrini, R. Broglia, A. Serani, and M. Diez, “Comparing multi-index stochastic collocation and multi-fidelity stochastic radial basis functions for forward uncertainty quantification of ship resistance,” Engineering with Computers, vol. 39, no. 3, pp. 2209-2237, 2023. https://doi.org/10.1007/s00366-021-01588-0

[14] Y. Feng, O. El Moctar, and T. E. Schellin, “Parametric hull form optimization of containerships for minimum resistance in calm water and in waves,” Journal of Marine Science and Application, vol. 20, no. 4, pp. 670-693, 2021. https://doi.org/10.1007/s11804-021-00243-w

[15] M. A. Naji, S. El Filali, K. Aarika, E. H. Benlahmar, R. A. Abdelouhahid, and O. Debauche, “Machine

learning algorithms for breast cancer prediction and diagnosis," Procedia Computer Science, vol. 191, pp. 487-492, 2021. https://doi.org/10.1016/j.procs.2021.07.062

[16] A. Sharifi, "Yield prediction with machine learning algorithms and satellite images," Journal of the Science of Food and Agriculture, vol. 101, no. 3, pp. 891-896, 2021. https://doi.org/10.1002/jsfa.10696

[17] A. Bahramifar, H. Afshin, and M. Emami Tabrizi, "Optimized simulation of river flow rate using regression-based models," Acta Geophysica, vol. 71, no. 5, pp. 2481-2496, 2023. https://doi.org/10.1007/s11600-022-00976-4

[18] L. Huang, M. Li, T. Romu, A. Dolatshah, and G. Thomas, "Simulation of a ship operating in an open-water ice channel," Ships and Offshore Structures, vol. 16, no. 4, pp. 353-362, 2021. https://doi.org/10.1080/17445302.2020.1729595

[19] A. Nazemian, and P. Ghadimi, "Global optimization of trimaran hull form to get minimum resistance by slender body method," Journal of the Brazilian Society of Mechanical Sciences and Engineering, vol. 43, no. 5, pp. 1-20, 2021. https://doi.org/10.1007/s40430-020-02791-8

[20] W. Kusdiana, and I. M. Ariana, "Analysis of ship resistance based on horizontal placement of fin stabilizer using CFD software," International Review on Modelling and Simulations, vol. 15, no. 1, pp. 53-63, 2022. https://doi.org/10.15866/iremos.v15i1.20104

[21] F. S. Gharehchopogh, M. Namazi, L. Ebrahimi, and B. Abdollahzadeh, "Advances in sparrow search algorithm: a comprehensive survey," Archives of Computational Methods in Engineering, vol. 30, no. 1, pp. 427-455, 2023. https://doi.org/10.1007/s11831-022-09804-w

[22] L. Xu, S. Zhao, and T. Wang, "Aero-optic imaging deviation prediction based on ISSA-ELM," Optoelectronics Letters, vol. 19, no. 7, pp. 425-431, 2023. https://doi.org/10.1007/s11801-023-2141-y